LANGUAGE-IMAGE MODELS WITH 3D UNDERSTANDING

Anonymous authors
Paper under double-blind review

ABSTRACT

Multi-modal large language models (MLLMs) have shown incredible capabilities in a variety of 2D vision and language tasks. We extend MLLMs' perceptual capabilities to ground and reason about images in 3-dimensional space. To that end, we first develop a large-scale pretraining dataset for 2D and 3D called LV3D by combining multiple existing 2D and 3D recognition datasets under a common task formulation: as multi-turn question-answering. Next, we introduce a new MLLM named **CUBE-LLM** and pre-train it on LV3D. We show that pure data scaling makes a strong 3D perception capability without 3D-specific architectural design or training objectives. **CUBE-LLM** exhibits intriguing properties similar to LLMs: (1) **CUBE-LLM** can apply chain-of-thought prompting to improve 3D understanding from 2D context information. (2) **CUBE-LLM** can follow complex and diverse instructions and adapt to versatile input and output formats. (3) **CUBE-LLM** can be visually prompted such as 2D box or a set of candidate 3D boxes from specialists. Our experiments on outdoor benchmarks demonstrate that **CUBE-LLM** significantly outperforms existing baselines by 21.3 points of AP_{BEV} on the Talk2Car dataset for 3D grounded reasoning and 17.7 points on the DriveLM dataset for complex reasoning about driving scenarios, respectively. **CUBE-LLM** also shows competitive results in general MLLM benchmarks such as refCOCO for 2D grounding with (87.0) average score, as well as visual question answering benchmarks such as VQAv2, GQA, SQA, POPE, etc. for complex reasoning.

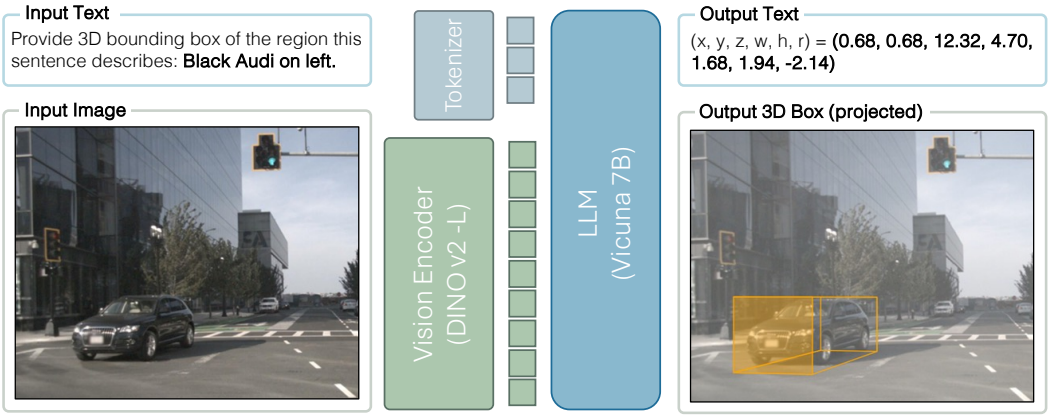

Figure 1: The overview of **CUBE-LLM** for 3D-grounding. The task requires a model to take an image, understand the input text prompt (e.g., "*Black Audi on left.*") and ground it in 3D space.

1 INTRODUCTION

Internet-scale visual data have brought forth the advent of multi-modal large language models (MLLMs). Rich and diverse visual supervision aligns pre-trained large language models with billions of parameters to visual modality. The best MLLMs can recognize, understand, and reason about images and videos far better than any of specially designed architectures and algorithms (gpt; Team et al., 2023). The decades worth of computer vision datasets —image classification, captioning, object detection, grounding, document parsing, optical character recognition (OCR)— fuels the powerful MLLMs through joint training as a next token prediction task. Introducing the ability to

"ground" in 2-dimensional space (*image coordinates*) bridges the low-level perception to high-level reasoning about visual input, much like human cognition. However, one critical difference is that we perceive the world in 3-dimensional space (*view coordinates*). This 3-dimensional grounding allows us to perceive and reason about the visual input closer to the actual world, which the current state of MLLMs has not explored yet.

In this work, our goal is to develop a framework to train an MLLM capable of reasoning in both 2D and 3D spaces. We demonstrate that pure data scaling can achieve our goal without any 3D-specific architectural design or training objective. We instead focus on careful data curation to address one question: *what tasks will induce 2D to 3D generalization?* To this end, we introduce a large-scale language-image pretraining dataset for 2D and 3D, called LV3D. We start by combining a diverse collection of 2D and 3D vision datasets for indoors and outdoors and standardize labels to follow the consistent format across datasets. We blend in the vision datasets with instruction-following data of MLLM training as a series of question-answer pairs (§ 3.1). Next, we augment our blended datasets by decomposing the vision labels into easier tasks (*e.g., 3D box* → *2D point, depth, size, orientation*). This trains our model to adapt to versatile input and output formats and connects the underlying 2D and 3D structure (§ 3.2). Most importantly, we mix in a series of QA pairs about an object for "step-by-step" reasoning, from easier (*e.g., 2D box*) to harder (*e.g., 3D box*) tasks. This directly induces 2D to 3D generalization due to the autoregressive nature of MLLMs (§ 3.3). Finally, we train a MLLM on LV3D as a single "next token prediction" task, called **CUBE-LLM** (§ 3.4).

CUBE-LLM exhibits several intriguing properties. First, **CUBE-LLM** can self-improve its 3D reasoning performance by prompting with its own 2D predictions. This *visual chain-of-thought reasoning* resembles the well-known behavior of LLMs (Wei et al., 2022b). Second, **CUBE-LLM** can adapt to versatile input and output formats and questions, which follows *instruction following* ability of LLMs (Wei et al., 2022a). Finally, **CUBE-LLM** can be *prompted* with any specialist models for any additional modalities (*e.g., LiDAR*) by simply adding their predictions to the question. **CUBE-LLM** shows remarkable improvement with data-scaling in both 2D and 3D, for indoor and outdoor scene grounding as well as complex reasoning tasks such as QA in driving scenarios.

We evaluate our model's performance in both 3D grounding and 3D complex reasoning tasks on various indoor and outdoor datasets as well as a standard MLLM benchmark and show qualitative results in 3D grounding in non-driving scenes (Fig. 2). For 3D grounding on the Talk2Car dataset (Deruyttere et al., 2019), **CUBE-LLM** surpasses the baselines by **21.3** in Bird's Eye View (BEV) AP (71.4 vs 50.1) and by **18.7** in 3D AP (64.1 vs 45.4). Additionally, our training framework improves the performance of **CUBE-LLM** on the DriveLM (Sima et al., 2023) dataset, nearly doubling the performance in the BEV AP (66.0 vs 33.2) for 3D grounding from a baseline. We also test **CUBE-LLM** on complex reasoning benchmark of driving scenarios (DriveLM), and improve the overall score by **17.7** (50.1 vs 32.4) compared to DriveLM baseline (Sima et al., 2023). Furthermore, we show that **CUBE-LLM** performs the state-of-the-art in 2D referring expression comprehension, achieving the average score of **87.0** on refCOCO/+/g. Finally, we show that **CUBE-LLM** maintains competitive performance in various MLLM benchmarks including VQAv2, GQA, etc., confirming that our 3D reasoning capability is an *expansion*, not a *trade-off*.

2 RELATED WORK

Vision Language Models. By scaling up pre-training on the internet-scale dataset, there has been significant progress for VLMs in the 2D vision-language domain, showing strong capabilities in few-shot generalization. VLBRRT (Su et al., 2020) and ViLBERT (Lu et al., 2019) capitalized on a BERT-style framework for image-text co-embedding. CLIP (Radford et al., 2021) embedded images and text captions into a shared feature space via contrastive learning and pioneered zero-shot vision tasks. BLIP (Li et al., 2022) and BLIP2 (Li et al., 2023a) further improved CLIP by leveraging extra pseudo-labeled data and better image/language encoders. Flamingo (Alayrac et al., 2022) and its open-source implementation Open-Flamingo (Awadalla et al., 2023) proposed a fast adaptation approach to enable in-context few-shot learning on novel visual-language tasks. GPT4V (gpt) and Gemini (Team et al., 2023) further demonstrated state-of-the-art human-level visual reasoning ability through scaling. LLaVA (Liu et al., 2023b) pioneered instruction fine-tuning in the multimodal field. These works have predominantly focused on 2D vision and language tasks. On the other hand,

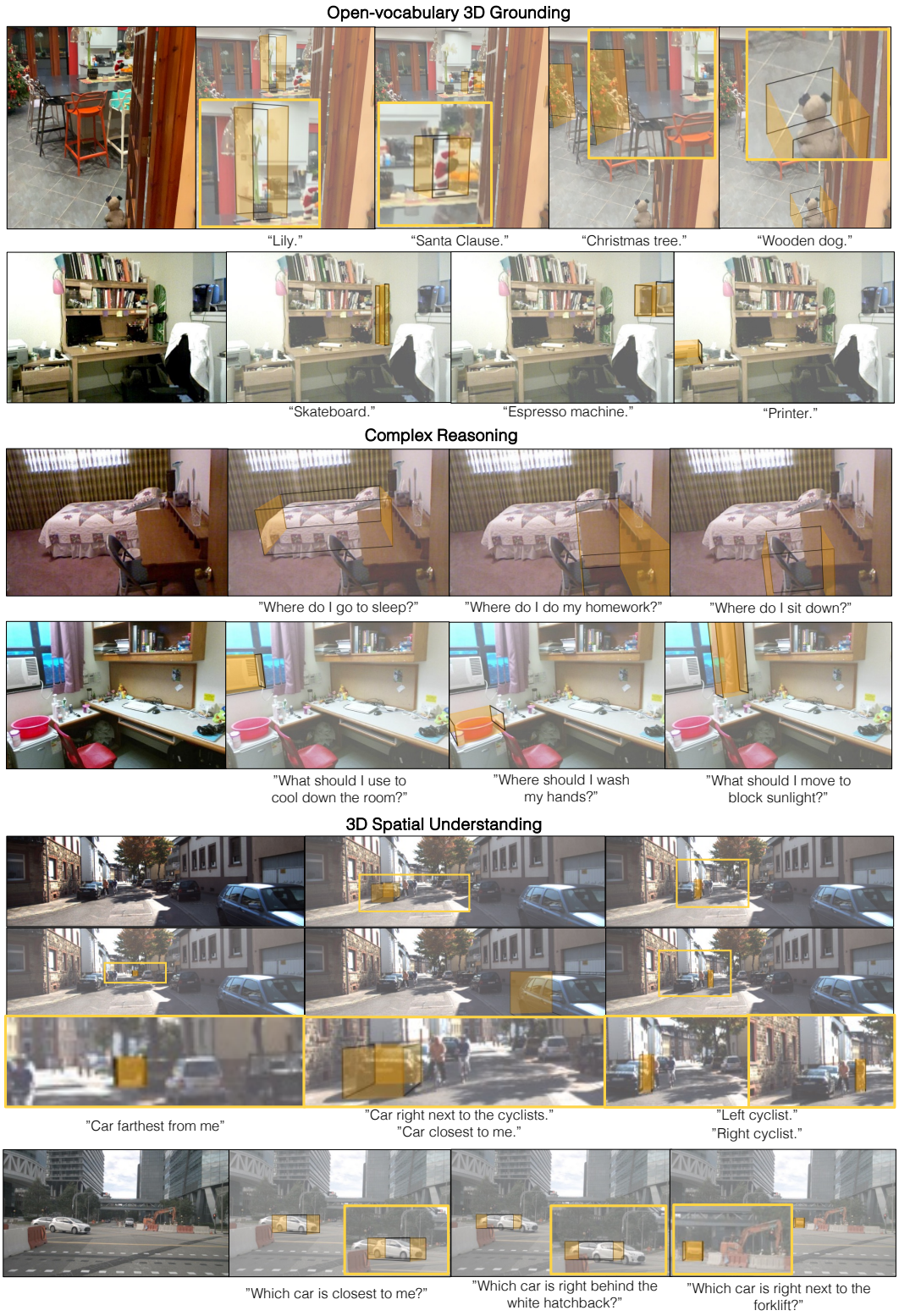

Figure 2: **Qualitative results** of **CUBE-LLM** 3D grounding: *open-vocabulary understanding* (**top**), *complex reasoning* (**middle**), and *3D spatial understanding* (**bottom**). Best viewed in color, **zoomed**.

we aim to adapt these MLLMs to enhance their capabilities for complex 3D reasoning and scene understanding tasks.

Image-grounded Reasoning. With the advancement of multi-modal large language models, image-grounded reasoning (referring and grounding) has shown great progress in 2D space. Image-grounded reasoning requires a model to localize an object or a region that an input prompt enquires or describes about a region of interest. VisionLLM (Wang et al., 2024b) adapts a 2D object detector to align with an LLM, and GPT4-ROI (Zhang et al., 2023b) employs hierarchical feature modeling of detectors to reason about input visual prompt (ROI). Kosmos-2 (Peng et al., 2023) and Shikra (Chen et al., 2023b) have shown pure transformer-based visual encoder can surpass using 2D detectors with data scaling. Recently, Ferret (You et al., 2023) has shown remarkable image-grounded reasoning from both free-form visual prompts and text prompts. In addition, Set-of-Mark (Yang et al., 2023) shows using visual marks on image from specialists allows frontier MLLM (gpt) to do image-grounded reasoning well. These works reason in 2D space (image coordinate). To the best of our knowledge, our work is the first to expand the reasoning capability of a MLLM to 3-dimensional space.

3 Unified Language-Image Pretraining for 2D and 3D

Our goal is to expand the capabilities of vision-language models to reason in 3-dimensional space. We propose a unified training framework to learn from both 2D and 3D perceptual data as well as standard image-text pairs. In this section, we first discuss the data standardization to train a vision-language model at scale (Sec. 3.1), task scaling to understand perceptual information in versatile I/O format (Sec. 3.2), *visual chain-of-thought* reasoning for 3D grounding and question answering tasks (Sec. 3.3), and finally, we present **Cube-LLM**, the final model of our unified training framework built on LLaVA-1.5 (Liu et al., 2023a) (Sec. 3.4).

3.1 Data-scaling for Image-based 3D Reasoning

Our goal is to train a single 2D + 3D MLLM from all data sources available. To standardize many different 2D and 3D grounding tasks into one, we standardize the data, phrase all tasks as next token prediction, and format 3D reasoning as a multi-turn conversation.

Data standardization. We consider points and boxes as our main spatial representation for 2D and 3D reasoning. We convert every label to either a point $o^{\text{2D}}_{\text{point}} = [\hat{x}, \hat{y}]$ or a bounding box $o^{\text{2D}}_{\text{box}} = [\hat{x}, \hat{y}, \hat{x}', \hat{y}']$. Similarly, we convert every 3D label to either $o^{\text{3D}}_{\text{point}} = [x, y, z]$ or $o^{\text{3D}}_{\text{box}} = [x, y, z, w, h, l, r_1, r_2, r_3]$ where r_1, r_2, r_3 are Euler angles. We first standardize image-based 3D datasets by unifying camera parameters. We follow the procedure of Omni3D (Brazil et al., 2023); define a virtual camera with a fixed focal length f and transform depth z according to the original camera parameters and the target image size. Since all 3D labels are unified to a consistent camera intrinsic, we can now convert all x and y coordinates to 2D projected coordinates $(\hat{x}, \hat{y})$. Consequently, we can represent all label formats to naturally follow 2D to 3D per-object token sequence:

$$o^{\textbf{2D}}_{\text{point}} = [\hat{x}, \hat{y}] \tag{1}$$

$$o^{\textbf{2D}}_{\text{box}} = [\hat{x}, \hat{y}, \hat{x}', \hat{y}'] \tag{2}$$

$$o^{\textbf{3D}}_{\text{point}} = [\hat{x}, \hat{y}, z] \tag{3}$$

$$o^{\textbf{3D}}_{\text{box}} = [\hat{x}, \hat{y}, z, w, h, l, r_1, r_2, r_3] \tag{4}$$

where each value is represented as a short sequence of text tokens (3 for 3-decimal numbers). This allows the model to predict consistent ordering of token sequence from 2D to 3D, which improves the understanding of the underlying structure. With autoregressive models, we first localize objects in image coordinates $(\hat{x}, \hat{y})$, then infer depth (z), and then infer the size and orientation (w, h, l, r_1, r_2, r_3).

3D reasoning as multi-turn conversations. Now, we combine the 2D and 3D data with language-image instruction tuning data of visual language models (Liu et al., 2023b). For each image and a set of object labels pair, we construct a multi-turn conversational question-answer data ($\mathbf{Q}_1$, $\mathbf{A}_1$, $\mathbf{Q}_2$, $\mathbf{A}_2$, $\ldots$, $\mathbf{Q}_n$, $\mathbf{A}_n$). Each question refers an object with one property b_q and enquires b_a:

$$b_q, b_a \in \{\text{box}_{\text{2D}}, \text{caption}, \text{box}_{\text{3D}}\} \tag{5}$$

Each object property has a set of prompts predefined, such as "`Provide the 3D bounding box of the region this sentence describes: <caption>`" for b_q = caption

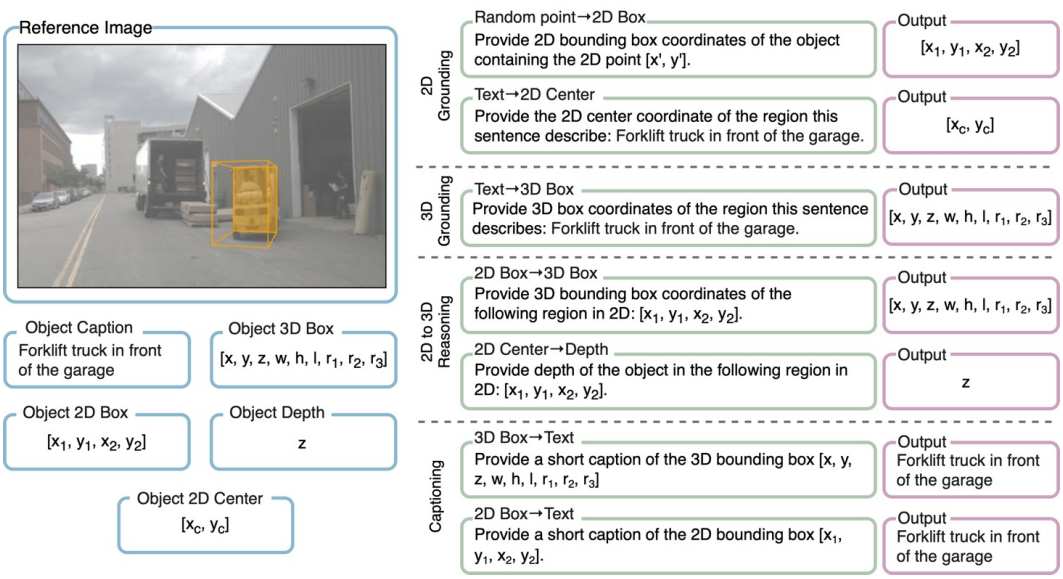

Figure 3: **Task-scaling for versatile I/O format.** Decomposing the existing label formats for 3D grounding task. A complete 3D location can be decomposed into a center point (`[x, y, z]`), a depth (`[z]`), a (projected) 2D point (`[xc, yc]`), and a (projected) 2D box (`[x1, y1, x2, y2]`). We define various tasks that connect among these to train versatile I/O formats. **Left**: available (decomposed) annotations. **Right**: various tasks for training.

and $b_a = \text{box}_{\text{3D}}$. We combine the meta information of objects (e.g., attribute, physical state, etc.) with the class name to enrich the textual information.

3.2 Task-scaling for Versatile I/O Format

We are interested in a generalist model that accepts input and generates output in versatile formats. Users may want to supplement 2D points or boxes as visual prompts during inference, or may only want the metric depth of an object instead of a complete 3D location. This interest in versatile I/O format shares the same spirit of instruction tuning in 2D-based visual language models (Liu et al., 2023b; Dai et al., 2023; Alayrac et al., 2022). To this end, we define multiple relevant tasks for a model to adapt to a wider spectrum of similar tasks in 2D and 3D. We start by *decomposing* the existing label formats to easier tasks as illustrated in Figure 3. After, we have expanded the set of object properties to construct question-answer pairs:

$$b_q \in \{\text{point}_{\text{2D}}, \text{box}_{\text{2D}}, \text{caption}, \text{point}_{\text{3D}}, \text{box}_{\text{3D}}\} \tag{6}$$

$$b_a \in \{\text{point}_{\text{2D}}, \text{box}_{\text{2D}}, \text{caption}, \text{depth}, \text{point}_{\text{3D}}, \text{box}_{\text{3D}}\} \tag{7}$$

We construct up to $n = 30$ question answer pairs $(\mathbf{Q}_{b_a}^{b_q}, \mathbf{A}_{b_a})$ sampled at random for each data. We combine a collection of 2D and 3D vision datasets (LV3D), summarized in Table 1, and jointly train with this expanded set of tasks.

3.3 Visual Chain-of-Thought Prompting

One of the most intriguing properties of large language models is its *emergent* ability to improve reasoning with intermediate steps (Wei et al., 2022b). This mostly attributes to a vast corpus of rich text data with numerous step-by-step question-answering samples (Wei et al., 2022a). We artificially supplement this *step-by-step* reasoning of 3D by interleaving multiple questions of the same object from easy-to-hard order (the left part of Figure. 4):

$$\text{maximize} \quad \begin{cases} p(\mathbf{A}_{\text{box}_{\text{2D}}} | \mathbf{Q}_{\text{box}_{\text{2D}}}^{\text{caption}}) & \textit{question 1} \\ p(\mathbf{A}_{\text{box}_{\text{3D}}} | \mathbf{Q}_{\text{box}_{\text{2D}}}^{\text{caption}}, \mathbf{A}_{\text{box}_{\text{2D}}}, \mathbf{Q}_{\text{box}_{\text{3D}}}^{\text{caption}}) & \textit{question 2} \\ \quad \ldots \end{cases} \tag{8}$$

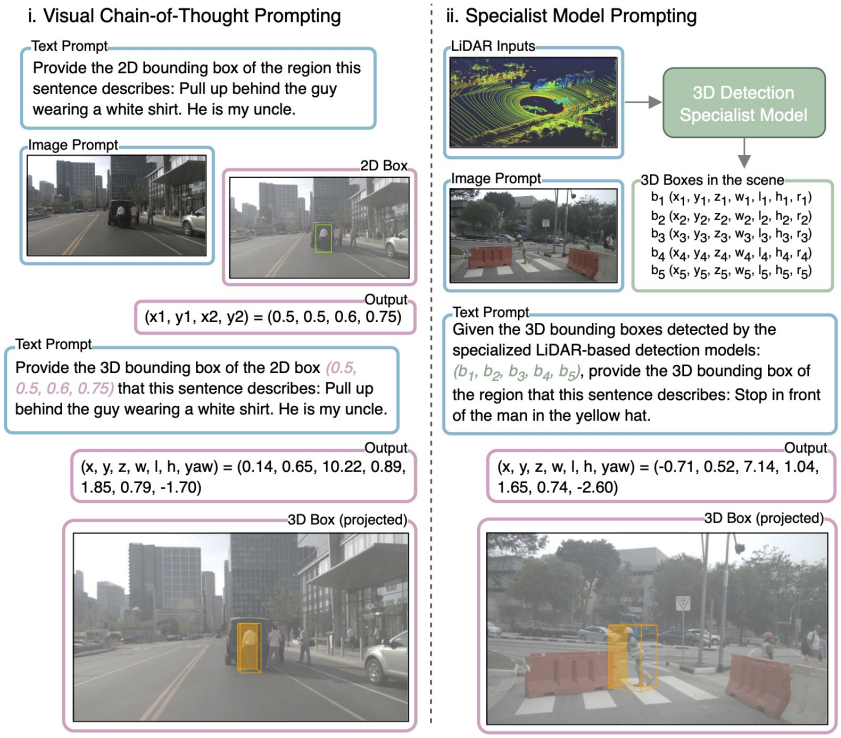

Figure 4: **CUBE-LLM inference with prompting**. **Left**: Visual Chain-of-Thought Prompting to reason in 3D step-by-step. **Right**: Incorporating specialist models to further improve localization of **CUBE-LLM**. Our model can either predict directly from text prompts, with visual chain-of-thought prompting, or with specialist predictions as prompts. Figure 9 and 10 in appendix visualize these.

Furthermore, we allow test-time adaptation to any specialist models by mixing in *candidate* objects as a system prompt (the right part of Figure. 4). This effectively alleviates the problem of localizing in 3D to "choosing the appropriate box from candidates",

$$\text{maximize} \quad p(\mathbf{A}_{\text{box}_{3\text{D}}} | \mathbf{S}_{\text{box}_{3\text{D}}}, \mathbf{Q}^{\text{caption}}_{\text{box}_{3\text{D}}}) \tag{9}$$

where $\mathbf{S}_{\text{box}_{3\text{D}}}$ is a set of candidate boxes, which can be provided by any specialist models (depending on available input modalities) at inference. During training, we use the ground truth boxes with a prompt `"Here is the list of 3D bounding boxes of all objects around the camera:"` and our model does not bind with any particular specialist model.

3.4 CUBE-LLM

We introduce **CUBE-LLM**, a multi-modal large language model based on LLaVA-1.5 architecture trained to reason in both 2D and 3D. Although we maintain the generality of model architecture, we make simple yet critical changes to the original LLaVA. We first replace the CLIP visual encoder with DINOv2 (Oquab et al., 2024) and undergo the same alignment step of the original LLaVA. Although DINOv2 is not a text-aligned visual encoder like CLIP, we found minimal degradation in the standard visual language model benchmarks while significantly improving 3D-related tasks. Then, we finetune the language model (Vicuna-7B (Chiang et al., 2023)) while freezing the visual encoder and jointly on LLaVA instruction-following data and the 2D part of LV3D following Sec. 3.1, 3.2 and 3.3. We use low image resolution (336×336) and train with a large batch size. Then, we proceed an additional finetuning stage for both visual and language models with high-resolution images (672×672) of the full LV3D. More details can be found in the section A and Figure 8 of the appendix.

4 EXPERIMENTS

We evaluate **CUBE-LLM** in three aspects: (1) 3D-grounded reasoning for indoor and outdoor scenes, (2) complex reasoning in 3D, and (3) standard MLLM benchmarks such as 2D grounding and VQA.

Table 1: **2D and 3D Language-Image Pretraining Dataset (LV3D)**. Summary of components detailing the number of images, tasks, availability of 2D and 3D labels, the number of QAs and objects, and their multiples during training (*stage 1* and *stage 2*). $\star$: Only used 2D bounding box.

dataset	images	labels_{2D}	labels_{3D}	captions	# QAs	stage 1	stage 2
LLaVA data (Liu et al., 2023b)	80K	✓	✗	✓	158K	1	0.5
refCOCO/+/g (Yu et al., 2016)	67K	✓	✗	✓	154K	1	0.5
GRIT (subset) (Peng et al., 2023)	4M	✓	✗	✓	6.9M	1	0.3
AS (filtered) (Wang et al., 2024a)	3.7M	✓	✗	✓	13.2M	1	0.5
COCO (Lin et al., 2014)	118K	✓	✗	✗	860K	1	0.5
Objects365 (Shao et al., 2019)	600K	✓	✗	✗	25.4M	0.3	0.2
SUN-RGBD (Song et al., 2015)	5K	✓	✓	✗	41K	$1^\star$	5
Hypersim (Roberts et al., 2021)	67K	✓	✓	✗	2M	$1^\star$	5
ArkitScenes (Baruch et al., 2021)	53K	✓	✓	✗	420K	$1^\star$	5
Objectron (Ahmadyan et al., 2021)	37K	✓	✓	✗	43K	$1^\star$	5
KITTI (Geiger et al., 2012)	4K	✓	✓	✗	25K	$1^\star$	5
NuScenes (Caesar et al., 2019)	40K	✓	✓	✗	1.1M	$1^\star$	2
Lyft (Houston et al., 2021)	105K	✓	✓	✗	723K	0	2
Argoverse2 (Wilson et al., 2021)	79K	✓	✓	✗	915K	0	4
Waymo (Sun et al., 2020)	680K	✓	✓	✗	5.1M	0	0.4
Total	9.6M	✓	✓	✓	40.9M	0.87	0.52

4.1 DATASETS

We pre-train **CUBE-LLM** on LV3D, a large collection of 2D and 3D dataset (Table 1). We format the existing labels into multi-turn instruction-following tasks under standard format, as described in Section 3.1, 3.2, and 3.3. We describe details of dataset construction in the section B of the appendix. We evaluate our model on diverse tasks, including the following 3D grounding datasets.

Talk2Car (Deruyttere et al., 2019) is a 3D referring expression comprehension dataset of various driving scenarios. It consists of 8,349 training samples and 1,163 validation samples with images and LiDAR data. It provides rich question-answer pairs grounded to an object in the image. Each object is labeled with a situational text that uniquely identifies the object (e.g., "*Wow hold on! That looks like my stolen bike over there! Drop me off next to it.*"). The original benchmark (Deruyttere et al., 2019) evaluates the 2D grounding performance with the $\text{AP}_{0.5}$ metric. MSSG (Cheng et al., 2023) extends the task to 3D grounding and evaluates on both BEV AP and 3D AP.

DriveLM (Sima et al., 2023) is a recently released question-answering dataset for driving scenarios based on NuScenes (Caesar et al., 2019). It consists of multi-view images and LiDAR point clouds as well as frame-level QA data, total of 4,871 frames. Each frame covers core AV tasks such as perception, prediction, and planning, as well as a scene description and 2D boxes of important objects. We process DriveLM and construct a 3D grounding dataset, which we call **DriveLM-Grounding**. We evaluate 3D grounding with the same BEV AP and 3D AP metric as those in Talk2Car. We also use the original **DriveLM-QA** data to fine-tune **CUBE-LLM** for complex reasoning tasks. We sample 600 scenes for training and 96 scenes for validation, which we include the DriveLM provided scenes for sample evaluation and Talk2Car validation split scenes.

The remaining details of the evaluation datasets will be in the section B of the appendix.

4.2 3D-GROUNDED REASONING

In Table 5, we show 2D and 3D grounding results of **CUBE-LLM** and baselines on Talk2Car dataset. The baselines that rely solely on camera inputs are only evaluated on 2D grounding, whereas those incorporating both camera and LiDAR inputs are evaluated on both 2D and 3D grounding. **CUBE-LLM** is pre-trained on LV3D and fine-tuned on Talk2Car with resolution 672×672. We apply a visual chain of thought when predicting the 3D grounding. Remarkably, our camera-only **CUBE-LLM** significantly surpasses the state-of-the-art model FA (Deruyttere et al., 2022) by 5.7 points on 2D $\text{AP}_{0.5}$. Surprisingly, **CUBE-LLM** also outperforms the camera+LiDAR baseline, Talk2Car-3D (Deruyttere et al., 2019), by 15.7 points on the BEV AP_A metric (Cheng et al., 2023). Our camera-only **CUBE-LLM** is only 3.8 points behind the state-of-the-art camera+LiDAR baseline MSSG (Cheng et al., 2023). MSSG (Cheng et al., 2023) utilized the LiDAR point encoder similar to CenterPoint (Yin et al., 2021) as well as image and text encoders for predicting 3D

Figure 5: **Talk2Car Benchmark for 2D and 3D Grounding**. We denote C as Camera and L as LiDAR. †: we use the top-30 predicted boxes of CenterPoint (Yin et al., 2021) as visual prompt as illustrated in Figure 4. AP_A and AP_B follow MSSG (Cheng et al., 2023) that apply different IoU threshold for each category. **Top**: Zeroshot Talk2Car result with varying LV3D data scale in %. **Bottom**: Zeroshot Talk2Car result with and without V-CoT training samples (Sec. 3.3) and 2D → 3D stage training (Sec. 3.4)

Method	Input	2D	BEV		3D	
		$AP_{0.5}$	AP_A	AP_B	AP_A	AP_B
2D Specialist						
Talk2Car-2D (Deruyttere et al., 2019)	C	50.5	-	-	-	-
VL-Bert (Su et al., 2020)	C	63.1	-	-	-	-
ViLBERT (Lu et al., 2019)	C	68.9	-	-	-	-
CMRT (Luo et al., 2020)	C	69.1	-	-	-	-
Stacked VLBert (Dai et al., 2020)	C	71.0	-	-	-	-
FA (Deruyttere et al., 2022)	C	73.5	-	-	-	-
CUBE-LLM ^{7b} (zero-shot)	C	49.2	32.0	19.5	22.3	9.8
CUBE-LLM ^{7b}	C	**79.2**	46.3	30.1	34.7	18.2
CUBE-LLM ^{13b} (zero-shot)	C	54.9	35.9	23.6	26.1	10.7
3D Specialist						
Talk2Car-3D (Deruyttere et al., 2019)	L + C	-	30.6	24.4	27.9	19.1
MSSG (Cheng et al., 2023)	L + C	-	50.1	35.7	45.4	23.7
CUBE-LLM ^{7b,†}	L + C	76.3	**71.4**	**61.2**	**64.1**	**39.8**

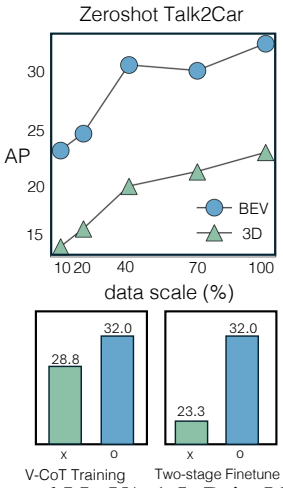

Table 2: **DriveLM QA and Grounding Benchmarks**. (**Left**) †: finetuned LLaVA-1.5. DriveLM baseline based on LLaMA Adapter V2 (Gao et al., 2023). **Top**: same split as the DriveLM baseline. **Bottom**: our larger test split held-out from all training. ‡: reported DriveLM result on the full test set. (**Right**) LV3D (2D) indicates that only 2D data in the pre-train dataset is included. We finetune **CUBE-LLM** and LLaVA-1.5 (Liu et al., 2023a) on the DriveLM-Grounding dataset.

(a) **DriveLM-QA**

Method	Acc.	Match	Overall
baseline split			
DriveLM baseline	0.0	28.3	32.4
LLaVA-1.5†	38.5	26.1	36.1
CUBE-LLM	**38.5**	**39.0**	**50.1**
our split			
DriveLM baseline‡	0.0	18.8	32.8
LLaVA-1.5†	24.1	36.4	43.8
CUBE-LLM	**32.4**	**39.2**	**45.4**

(b) **DriveLM-Grounding**

Method	AP_A^{BEV}	AP_B^{BEV}	AP_A^{3D}	AP_B^{3D}
finetune				
LLaVA-1.5	33.2	16.3	21.7	7.7
CLIP → DINOv2	39.6	21.7	25.8	10.5
+ LV3D (2D)	50.5	31.2	32.5	17.3
+ LV3D (3D)	**66.0**	**52.1**	**56.2**	**40.5**

grounding. Similarly, we leverage the LiDAR modality by using the top-30 predictions from CenterPoint (Yin et al., 2021) as input prompt of **CUBE-LLM**. We observe a substantial 25.1 points improvement in AP_A, outperforming MSSG (Cheng et al., 2023) by 21.3 points. Furthermore, we observe a similar trend on the DriveLM-Grounding dataset, shown in Table 2. **CUBE-LLM** shows significant improvements compared to directly finetuning from LLaVA-1.5, resulting in a 32.8 points improvement on the BEV AP_A metric. Lastly, we show indoor 3D grounding in Table 3, where we compare **CUBE-LLM** trained with *LV3D-small* and LV3D. LV3D-small contains the same indoor 3D dataset but without the most of outdoor data. Under our training framework, outdoor data scaling translates to indoor well. We describe the detailed experiment setting in the section B of the appendix.

Ablations. In Figure 5 (right), we first show **CUBE-LLM** exhibits an impressive scalability in 3D grounding task. Next, we show that employing the visual chain-of-thought samples during training improves zeroshot 3D AP by 3.2 points. The process of V-CoT and Specialist Promptings are illustrated in Figure 6 or in Figure 9 and 10 in the appendix.

4.3 COMPLEX REASONING IN 3D

To show the effectiveness of 3D reasoning capability, we finetune **CUBE-LLM** on DriveLM-QA dataset (Table 2). We compare **CUBE-LLM** with LLaVA-1.5 (Liu et al., 2023a) to show the impact of our pretraining, as well as the official baseline (Sima et al., 2023). All models use 7-B scale LLM (Vicuna-7B (Chiang et al., 2023) or LLaMA-7B (Touvron et al., 2023)) and are fine-tuned on a subset

Table 3: **Indoor 3D Grounding Benchmark.** Here we compare **CUBE-LLM** trained on "small" subset of LV3D and the full LV3D. Although the subset and full LV3D share the same indoor datasets, the added 2D data and outdoor 3D data translate to better indoor 3D grounding result.

Pre-train Data	Objectron		ArkitScenes		SUN-RGBD	
	mAP_{3D}^{cls}	$mAP_{3D}^{cls+loc}$	mAP_{3D}^{cls}	$mAP_{3D}^{cls+loc}$	mAP_{3D}^{cls}	$mAP_{3D}^{cls+loc}$
LV3D-small	56.7	36.1	21.6	28.3	25.5	25.5
LV3D	69.8	45.4	23.5	31.8	29.7	28.8
Δ	**13.1**	**9.3**	**1.9**	**3.5**	**4.2**	**3.3**

Table 4: **Referring Expression Comprehension Benchmark**. We compare **CUBE-LLM** with other MLLMs for general 2D grounding tasks. **CUBE-LLM** consistently performs best in all data splits.

Models	Size	RefCOCO			RefCOCO+			RefCOCOg		
		val	testA	testB	val	testA	testB	val	test	Avg.
Specialist										
MAttNet (Yu et al., 2018)		76.4	80.4	69.3	64.9	70.3	56.0	66.7	67.0	68.9
OFA-L (Wang et al., 2022)		80.0	83.7	76.4	68.3	76.0	61.8	67.6	67.6	72.7
TransVG (Deng et al., 2021)		81.0	82.7	78.4	64.8	70.7	56.9	68.7	67.7	71.4
UNITER (Chen et al., 2020)		81.4	87.0	74.2	75.9	81.5	66.7	74.0	68.7	76.2
VILLA (Gan et al., 2020)		82.4	87.5	74.8	76.2	81.5	66.8	76.2	76.7	77.8
UniTAB (Yang et al., 2022)		86.3	88.8	80.6	78.7	83.2	69.5	80.0	80.0	80.6
MDETR (Kamath et al., 2021)		86.8	89.6	81.4	79.5	84.1	70.6	81.6	80.9	81.8
Grounding DINO L (Liu et al., 2023c)		90.6	93.2	88.2	82.8	89.0	75.9	86.1	87.0	86.6
Generalist										
LLaVA-1.5 (Liu et al., 2023a)	7B	75.6	82.1	66.9	65.5	76.2	53.9	68.9	69.1	69.8
VisionLLM-H (Wang et al., 2024b)	7B	86.7	-	-	-	-	-	-	-	-
Shikra (Chen et al., 2023b)	7B	87.0	90.6	80.2	81.6	87.4	72.1	82.3	82.2	82.9
Ferret (You et al., 2023)	7B	87.5	91.4	82.5	80.8	87.4	73.1	83.9	84.8	83.9
MiniGPT-v2 (Chen et al., 2023a)	7B	88.7	91.7	85.3	80.0	85.1	74.5	84.4	84.7	83.8
LLaVA-G (Zhang et al., 2023a)	7B	89.2	-	-	81.7	-	-	84.8	-	-
Qwen-VL (Bai et al., 2023)	7B	88.6	92.3	84.5	82.8	88.6	76.8	86.0	86.3	85.7
CUBE-LLM	7B	**90.9**	**92.6**	**87.9**	**83.9**	**89.2**	**77.4**	**86.6**	**87.2**	**87.0**
Shikira (Chen et al., 2023b)	13B	87.8	91.1	81.8	82.9	87.8	74.4	82.6	83.2	84.0
Ferret (You et al., 2023)	13B	89.5	92.4	84.4	82.8	88.1	75.2	85.8	86.3	85.6
CUBE-LLM	13B	**91.8**	**93.5**	**88.6**	**86.0**	**90.8**	**79.1**	**87.6**	**88.6**	**88.3**

Table 5: **MLLM Benchmarks**. We compare **CUBE-LLM** in various general MLLM tasks.

Model	Size	VQA^{v2}	GQA	VizWiz	SQA^{I}	POPE
BLIP-2 (Li et al., 2023a)	13B	41.0	41.0	19.6	61.0	85.3
InstructBLIP (Dai et al., 2023)	7B	-	49.2	34.5	60.5	-
InstructBLIP (Dai et al., 2023)	13B	-	49.5	33.4	63.1	78.9
IDEFICS (Laurençon et al., 2023)	9B	50.9	38.4	35.5	-	-
Shikra (Chen et al., 2023b)	13B	77.4	-	-	-	-
Qwen-VL (Bai et al., 2023)	7B	78.8	59.3	35.2	67.1	-
Qwen-VL (chat) (Bai et al., 2023)	7B	78.2	57.5	38.9	68.2	-
miniGPT-v2 (Chen et al., 2023a)	7B	-	60.1	**53.6**	-	-
LLaVA-1.5 (Liu et al., 2023a)	7B	78.5	62.0	50.0	66.8	85.9
LLaVA-1.5 (Liu et al., 2023a)	13B	**80.0**	63.3	53.6	71.6	85.9
CUBE-LLM	7B	78.3	62.4	51.0	69.2	87.1
CUBE-LLM	13B	79.9	**64.1**	53.0	**72.2**	**88.2**

of DriveLM train split. The top rows are the result of scenes held out by the authors and the bottom rows are our additional split to evaluate models on a larger test set. The evaluation metric is based on accuracy, match (localization), BLEU/$ROUGE_L$/CIDEr, and ChatGPT score for favorable text generation. In Figure 7, we visualize **CUBE-LLM**'s prediction for complex reasoning in driving.

4.4 GENERAL MLLM BENCHMARKS

We show the performance of **CUBE-LLM** on general MLLM benchmarks. In Table 4, we compare **CUBE-LLM** to the state-of-the-arts in Referring Expression Comprehension (REC) benchmark on refCOCO/+/g (Yu et al., 2016) dataset. We compare **CUBE-LLM** to *specialist* models such as MDETR (Kamath et al., 2021) and UniTAB (Yang et al., 2022) which employs detection-specific architecture, and *generalist* models of same size such as Ferret (You et al., 2023), Qwen-VL (Bai et al.,

Figure 6: **CUBE-LLM inference with prompting**. **Left**: Visual Chain-of-Thought Prompting to reason in 3D step-by-step. **Right**: Incorporating specialist models to further improve localization of **CUBE-LLM**. Blue 3D boxes are the predictions of CenterPoint on corresponding LiDAR points.

Figure 7: **CUBE-LLM prediction on DriveLM-QA.** Orange marks are predicted 2D points by **CUBE-LLM**. Blue marks are the reference marks and the corresponding bounding box in the ground truth answers. Red circle is the predicted object that does not agree with the ground truth.

2023) and MiniGPT-v2 (Chen et al., 2023a). In all test splits, **CUBE-LLM** consistently outperforms with average score of **87.0**. In Table 5, we compare **CUBE-LLM** with other competitive MLLMs of same model size on VQAv2 (Goyal et al., 2017), GQA (Hudson & Manning, 2019), VizWiz (Gurari et al., 2018), ScienceQA-Image (Lu et al., 2022), and POPE (Li et al., 2023b). The first row has models with fully zero-shot evaluation, and the bottom rows have models that have seen images from some of the datasets. Compared to LLaVA-1.5 (Liu et al., 2023a), miniGPT-v2 (Chen et al., 2023a) and Qwen-VL (Bai et al., 2023), **CUBE-LLM** maintain the competitive result, validating that our 3D understanding does not degrade general reasoning capability of MLLM.

5 CONCLUSION

In this paper, we present **CUBE-LLM**, a multi-modal language model that can reason in both 2D and 3D. We provide a collection of datasets (LV3D) and a training framework to effectively scale MLLM training for 3D understanding. We evaluate **CUBE-LLM** in 2D and 3D grounded reasoning and VQA tasks, and show competitive results. We also show that **CUBE-LLM** exhibits the behaviors of LLMs such as chain-of-thought prompting or visual prompting to further improve the 3D localization of our model. Finally, we show that our model can adapt to any specialist models during inference by prompting their predictions as visual prompts. We examine that pure transformer-based MLLM with minimal inductive bias can learn about 3D understanding solely by data scaling.

REFERENCES

Openai chat. https://openai.com/research/gpt-4v-system-card. Accessed: 2023-10-20. 1, 2, 4

Adel Ahmadyan, Liangkai Zhang, Artsiom Ablavatski, Jianing Wei, and Matthias Grundmann. Objectron: A large scale dataset of object-centric videos in the wild with pose annotations. *CVPR*, 2021. 7, 16

Jean-Baptiste Alayrac, Jeff Donahue, Pauline Luc, Antoine Miech, Iain Barr, Yana Hasson, Karel Lenc, Arthur Mensch, Katie Millican, Malcolm Reynolds, Roman Ring, Eliza Rutherford, Serkan Cabi, Tengda Han, Zhitao Gong, Sina Samangooei, Marianne Monteiro, Jacob Menick, Sebastian Borgeaud, Andy Brock, Aida Nematzadeh, Sahand Sharifzadeh, Mikolaj Binkowski, Ricardo Barreira, Oriol Vinyals, Andrew Zisserman, and Karen Simonyan. Flamingo: a visual language model for few-shot learning. *ArXiv*, abs/2204.14198, 2022. URL https://api.semanticscholar.org/CorpusID:248476411. 2, 5, 19

Anas Awadalla, Irena Gao, Josh Gardner, Jack Hessel, Yusuf Hanafy, Wanrong Zhu, Kalyani Marathe, Yonatan Bitton, Samir Yitzhak Gadre, Shiori Sagawa, Jenia Jitsev, Simon Kornblith, Pang Wei Koh, Gabriel Ilharco, Mitchell Wortsman, and Ludwig Schmidt. Openflamingo: An open-source framework for training large autoregressive vision-language models. *ArXiv*, abs/2308.01390, 2023. URL https://api.semanticscholar.org/CorpusID:261043320. 2

Jinze Bai, Shuai Bai, Shusheng Yang, Shijie Wang, Sinan Tan, Peng Wang, Junyang Lin, Chang Zhou, and Jingren Zhou. Qwen-vl: A versatile vision-language model for understanding, localization, text reading, and beyond. *arXiv preprint arXiv:2308.12966*, 2023. 9, 10

Gilad Baruch, Zhuoyuan Chen, Afshin Dehghan, Tal Dimry, Yuri Feigin, Peter Fu, Thomas Gebauer, Brandon Joffe, Daniel Kurz, Arik Schwartz, and Elad Shulman. ARKitscenes - a diverse real-world dataset for 3d indoor scene understanding using mobile RGB-d data. In *NeurIPS Datasets and Benchmarks Track (Round 1)*, 2021. 7, 16

Garrick Brazil, Abhinav Kumar, Julian Straub, Nikhila Ravi, Justin Johnson, and Georgia Gkioxari. Omni3D: A large benchmark and model for 3D object detection in the wild. In *CVPR*, Vancouver, Canada, June 2023. IEEE. 4, 16

Holger Caesar, Varun Bankiti, Alex H. Lang, Sourabh Vora, Venice Erin Liong, Qiang Xu, Anush Krishnan, Yu Pan, Giancarlo Baldan, and Oscar Beijbom. nuscenes: A multimodal dataset for autonomous driving. *arXiv preprint arXiv:1903.11027*, 2019. 7

Jun Chen, Deyao Zhu, Xiaoqian Shen, Xiang Li, Zechu Liu, Pengchuan Zhang, Raghuraman Krishnamoorthi, Vikas Chandra, Yunyang Xiong, and Mohamed Elhoseiny. Minigpt-v2: large language model as a unified interface for vision-language multi-task learning. *arXiv preprint arXiv:2310.09478*, 2023a. 9, 10

Keqin Chen, Zhao Zhang, Weili Zeng, Richong Zhang, Feng Zhu, and Rui Zhao. Shikra: Unleashing multimodal llm's referential dialogue magic. *arXiv preprint arXiv:2306.15195*, 2023b. 4, 9

Yen-Chun Chen, Linjie Li, Licheng Yu, Ahmed El Kholy, Faisal Ahmed, Zhe Gan, Yu Cheng, and Jingjing Liu. Uniter: Universal image-text representation learning. In *European conference on computer vision*, pp. 104–120. Springer, 2020. 9

Wenhao Cheng, Junbo Yin, Wei Li, Ruigang Yang, and Jianbing Shen. Language-guided 3d object detection in point cloud for autonomous driving. *arXiv preprint arXiv:2305.15765*, 2023. 7, 8

Wei-Lin Chiang, Zhuohan Li, Zi Lin, Ying Sheng, Zhanghao Wu, Hao Zhang, Lianmin Zheng, Siyuan Zhuang, Yonghao Zhuang, Joseph E. Gonzalez, Ion Stoica, and Eric P. Xing. Vicuna: An open-source chatbot impressing gpt-4 with 90%* chatgpt quality, March 2023. URL https://lmsys.org/blog/2023-03-30-vicuna/. 6, 8

Hang Dai, Shujie Luo, Yong Ding, and Ling Shao. Commands for autonomous vehicles by progressively stacking visual-linguistic representations. In *ECCV Workshops*, 2020. 8

Wenliang Dai, Junnan Li, Dongxu Li, Anthony Meng Huat Tiong, Junqi Zhao, Weisheng Wang, Boyang Albert Li, Pascale Fung, and Steven C. H. Hoi. Instructblip: Towards general-purpose vision-language models with instruction tuning. *ArXiv*, abs/2305.06500, 2023. URL https://api.semanticscholar.org/CorpusID:258615266. 5, 9, 19

Jiajun Deng, Zhengyuan Yang, Tianlang Chen, Wen gang Zhou, and Houqiang Li. Transvg: End-to-end visual grounding with transformers. *2021 IEEE/CVF International Conference on Computer Vision (ICCV)*, pp. 1749–1759, 2021. URL https://api.semanticscholar.org/CorpusID:233296838. 9

Thierry Deruyttere, Simon Vandenhende, Dusan Grujicic, Luc Van Gool, and Marie Francine Moens. Talk2car: Taking control of your self-driving car. In *Proceedings of the 2019 Conference on Empirical Methods in Natural Language Processing and the 9th International Joint Conference on Natural Language Processing (EMNLP-IJCNLP)*, pp. 2088–2098, 2019. 2, 7, 8

Thierry Deruyttere, Dusan Grujicic, Matthew B. Blaschko, and Marie-Francine Moens. Talk2car: Predicting physical trajectories for natural language commands. *IEEE Access*, 2022. 7, 8

Alexey Dosovitskiy, Lucas Beyer, Alexander Kolesnikov, Dirk Weissenborn, Xiaohua Zhai, Thomas Unterthiner, Mostafa Dehghani, Matthias Minderer, Georg Heigold, Sylvain Gelly, Jakob Uszkoreit, and Neil Houlsby. An image is worth 16x16 words: Transformers for image recognition at scale. *ICLR*, 2021. 15

Zhe Gan, Yen-Chun Chen, Linjie Li, Chen Zhu, Yu Cheng, and Jingjing Liu. Large-scale adversarial training for vision-and-language representation learning. *Advances in Neural Information Processing Systems*, 33:6616–6628, 2020. 9

Peng Gao, Jiaming Han, Renrui Zhang, Ziyi Lin, Shijie Geng, Aojun Zhou, Wei Zhang, Pan Lu, Conghui He, Xiangyu Yue, Hongsheng Li, and Yu Qiao. Llama-adapter v2: Parameter-efficient visual instruction model. *arXiv preprint arXiv:2304.15010*, 2023. 8

Andreas Geiger, Philip Lenz, and Raquel Urtasun. Are we ready for autonomous driving? the kitti vision benchmark suite. In *CVPR*, 2012. 7

Yash Goyal, Tejas Khot, Douglas Summers-Stay, Dhruv Batra, and Devi Parikh. Making the v in vqa matter: Elevating the role of image understanding in visual question answering. In *Proceedings of the IEEE conference on computer vision and pattern recognition*, pp. 6904–6913, 2017. 10

Danna Gurari, Qing Li, Abigale J Stangl, Anhong Guo, Chi Lin, Kristen Grauman, Jiebo Luo, and Jeffrey P Bigham. Vizwiz grand challenge: Answering visual questions from blind people. In *Proceedings of the IEEE conference on computer vision and pattern recognition*, pp. 3608–3617, 2018. 10

John Houston, Guido Zuidhof, Luca Bergamini, Yawei Ye, Long Chen, Ashesh Jain, Sammy Omari, Vladimir Iglovikov, and Peter Ondruska. One thousand and one hours: Self-driving motion prediction dataset. In *Conference on Robot Learning*, pp. 409–418. PMLR, 2021. 7, 16

Drew A Hudson and Christopher D Manning. Gqa: A new dataset for real-world visual reasoning and compositional question answering. In *Proceedings of the IEEE/CVF conference on computer vision and pattern recognition*, pp. 6700–6709, 2019. 10

Aishwarya Kamath, Mannat Singh, Yann LeCun, Gabriel Synnaeve, Ishan Misra, and Nicolas Carion. Mdetr-modulated detection for end-to-end multi-modal understanding. In *Proceedings of the IEEE/CVF International Conference on Computer Vision*, pp. 1780–1790, 2021. 9

Alexander Kirillov, Eric Mintun, Nikhila Ravi, Hanzi Mao, Chloe Rolland, Laura Gustafson, Tete Xiao, Spencer Whitehead, Alexander C Berg, Wan-Yen Lo, et al. Segment anything. In *Proceedings of the IEEE/CVF International Conference on Computer Vision*, pp. 4015–4026, 2023. 16

Hugo Laurençon, Lucile Saulnier, Léo Tronchon, Stas Bekman, Amanpreet Singh, Anton Lozhkov, Thomas Wang, Siddharth Karamcheti, Alexander M. Rush, Douwe Kiela, Matthieu Cord, and Victor Sanh. Obelics: An open web-scale filtered dataset of interleaved image-text documents, 2023. 9

Junnan Li, Dongxu Li, Caiming Xiong, and Steven Hoi. Blip: Bootstrapping language-image pre-training for unified vision-language understanding and generation. In *ICML*, 2022. 2

Junnan Li, Dongxu Li, Silvio Savarese, and Steven Hoi. BLIP-2: bootstrapping language-image pre-training with frozen image encoders and large language models. In *ICML*, 2023a. 2, 9

Yifan Li, Yifan Du, Kun Zhou, Jinpeng Wang, Wayne Xin Zhao, and Ji-Rong Wen. Evaluating object hallucination in large vision-language models. In *The 2023 Conference on Empirical Methods in Natural Language Processing*, 2023b. URL https://openreview.net/forum?id=xozJw0kZXF. 10

Tsung-Yi Lin, Michael Maire, Serge Belongie, James Hays, Pietro Perona, Deva Ramanan, Piotr Dollár, and C Lawrence Zitnick. Microsoft coco: Common objects in context. In *Computer Vision–ECCV 2014: 13th European Conference, Zurich, Switzerland, September 6-12, 2014, Proceedings, Part V 13*, pp. 740–755. Springer, 2014. 7

Haotian Liu, Chunyuan Li, Yuheng Li, and Yong Jae Lee. Improved baselines with visual instruction tuning, 2023a. 4, 8, 9, 10, 15

Haotian Liu, Chunyuan Li, Qingyang Wu, and Yong Jae Lee. Visual instruction tuning. In *NeurIPS*, 2023b. 2, 4, 5, 7

Shilong Liu, Zhaoyang Zeng, Tianhe Ren, Feng Li, Hao Zhang, Jie Yang, Chunyuan Li, Jianwei Yang, Hang Su, Jun Zhu, et al. Grounding dino: Marrying dino with grounded pre-training for open-set object detection. *arXiv preprint arXiv:2303.05499*, 2023c. 9

Jiasen Lu, Dhruv Batra, Devi Parikh, and Stefan Lee. Vilbert: Pretraining task-agnostic visiolinguistic representations for vision-and-language tasks. *Advances in neural information processing systems*, 32, 2019. 2, 8

Pan Lu, Swaroop Mishra, Tony Xia, Liang Qiu, Kai-Wei Chang, Song-Chun Zhu, Oyvind Tafjord, Peter Clark, and Ashwin Kalyan. Learn to explain: Multimodal reasoning via thought chains for science question answering. In *The 36th Conference on Neural Information Processing Systems (NeurIPS)*, 2022. 10

Shujie Luo, Hang Dai, Ling Shao, and Yong Ding. C4av: Learning cross-modal representations from transformers. In *ECCV Workshops*, 2020. 8

Maxime Oquab, Timothée Darcet, Théo Moutakanni, Huy V. Vo, Marc Szafraniec, Vasil Khalidov, Pierre Fernandez, Daniel HAZIZA, Francisco Massa, Alaaeldin El-Nouby, Mido Assran, Nicolas Ballas, Wojciech Galuba, Russell Howes, Po-Yao Huang, Shang-Wen Li, Ishan Misra, Michael Rabbat, Vasu Sharma, Gabriel Synnaeve, Hu Xu, Herve Jegou, Julien Mairal, Patrick Labatut, Armand Joulin, and Piotr Bojanowski. DINOv2: Learning robust visual features without supervision. *Transactions on Machine Learning Research*, 2024. ISSN 2835-8856. URL https://openreview.net/forum?id=a68SUt6zFt. 6

Zhiliang Peng, Wenhui Wang, Li Dong, Yaru Hao, Shaohan Huang, Shuming Ma, and Furu Wei. Kosmos-2: Grounding multimodal large language models to the world. *arXiv preprint arXiv:2306.14824*, 2023. 4, 7, 16

Alec Radford, Jong Wook Kim, Chris Hallacy, Aditya Ramesh, Gabriel Goh, Sandhini Agarwal, Girish Sastry, Amanda Askell, Pamela Mishkin, Jack Clark, et al. Learning transferable visual models from natural language supervision. In *International conference on machine learning*, pp. 8748–8763. PMLR, 2021. 2

Mike Roberts, Jason Ramapuram, Anurag Ranjan, Atulit Kumar, Miguel Angel Bautista, Nathan Paczan, Russ Webb, and Joshua M. Susskind. Hypersim: A photorealistic synthetic dataset for holistic indoor scene understanding. In *ICCV*, 2021. 7

Shuai Shao, Zeming Li, Tianyuan Zhang, Chao Peng, Gang Yu, Xiangyu Zhang, Jing Li, and Jian Sun. Objects365: A large-scale, high-quality dataset for object detection. In *2019 IEEE/CVF International Conference on Computer Vision (ICCV)*, 2019. 7

Chonghao Sima, Katrin Renz, Kashyap Chitta, Li Chen, Hanxue Zhang, Chengen Xie, Ping Luo, Andreas Geiger, and Hongyang Li. Drivelm: Driving with graph visual question answering. *arXiv preprint arXiv:2312.14150*, 2023. 2, 7, 8, 17

Shuran Song, Samuel P Lichtenberg, and Jianxiong Xiao. Sun rgb-d: A rgb-d scene understanding benchmark suite. In *CVPR*, 2015. 7, 16

Weijie Su, Xizhou Zhu, Yue Cao, Bin Li, Lewei Lu, Furu Wei, and Jifeng Dai. Vl-bert: Pre-training of generic visual-linguistic representations. In *International Conference on Learning Representations*, 2020. URL https://openreview.net/forum?id=SygXPaEYvH. 2, 8

Pei Sun, Henrik Kretzschmar, Xerxes Dotiwalla, Aurelien Chouard, Vijaysai Patnaik, Paul Tsui, James Guo, Yin Zhou, Yuning Chai, Benjamin Caine, Vijay Vasudevan, Wei Han, Jiquan Ngiam, Hang Zhao, Aleksei Timofeev, Scott Ettinger, Maxim Krivokon, Amy Gao, Aditya Joshi, Yu Zhang, Jonathon Shlens, Zhifeng Chen, and Dragomir Anguelov. Scalability in perception for autonomous driving: Waymo open dataset. In *Proceedings of the IEEE/CVF Conference on Computer Vision and Pattern Recognition (CVPR)*, June 2020. 7, 16

Gemini Team, Rohan Anil, Sebastian Borgeaud, Yonghui Wu, Jean-Baptiste Alayrac, Jiahui Yu, Radu Soricut, Johan Schalkwyk, Andrew M Dai, Anja Hauth, et al. Gemini: a family of highly capable multimodal models. *arXiv preprint arXiv:2312.11805*, 2023. 1, 2

Hugo Touvron, Thibaut Lavril, Gautier Izacard, Xavier Martinet, Marie-Anne Lachaux, Timothée Lacroix, Baptiste Rozière, Naman Goyal, Eric Hambro, Faisal Azhar, et al. Llama: Open and efficient foundation language models. *arXiv preprint arXiv:2302.13971*, 2023. 8

Peng Wang, An Yang, Rui Men, Junyang Lin, Shuai Bai, Zhikang Li, Jianxin Ma, Chang Zhou, Jingren Zhou, and Hongxia Yang. Ofa: Unifying architectures, tasks, and modalities through a simple sequence-to-sequence learning framework. *CoRR*, abs/2202.03052, 2022. 9

Weiyun Wang, Yiming Ren, Haowen Luo, Tiantong Li, Chenxiang Yan, Zhe Chen, Wenhai Wang, Qingyun Li, Lewei Lu, Xizhou Zhu, et al. The all-seeing project v2: Towards general relation comprehension of the open world. *arXiv preprint arXiv:2402.19474*, 2024a. 7, 16

Wenhai Wang, Zhe Chen, Xiaokang Chen, Jiannan Wu, Xizhou Zhu, Gang Zeng, Ping Luo, Tong Lu, Jie Zhou, Yu Qiao, et al. Visionllm: Large language model is also an open-ended decoder for vision-centric tasks. *Advances in Neural Information Processing Systems*, 36, 2024b. 4, 9

Jason Wei, Maarten Bosma, Vincent Zhao, Kelvin Guu, Adams Wei Yu, Brian Lester, Nan Du, Andrew M. Dai, and Quoc V Le. Finetuned language models are zero-shot learners. In *International Conference on Learning Representations*, 2022a. URL https://openreview.net/forum?id=gEZrGCozdqR. 2, 5

Jason Wei, Xuezhi Wang, Dale Schuurmans, Maarten Bosma, Fei Xia, Ed Chi, Quoc V Le, Denny Zhou, et al. Chain-of-thought prompting elicits reasoning in large language models. *Advances in Neural Information Processing Systems*, 35:24824–24837, 2022b. 2, 5

Benjamin Wilson, William Qi, Tanmay Agarwal, John Lambert, Jagjeet Singh, Siddhesh Khandelwal, Bowen Pan, Ratnesh Kumar, Andrew Hartnett, Jhony Kaesemodel Pontes, Deva Ramanan, Peter Carr, and James Hays. Argoverse 2: Next generation datasets for self-driving perception and forecasting. In *Proceedings of the Neural Information Processing Systems Track on Datasets and Benchmarks (NeurIPS Datasets and Benchmarks 2021)*, 2021. 7, 16

Jianwei Yang, Hao Zhang, Feng Li, Xueyan Zou, Chunyuan Li, and Jianfeng Gao. Set-of-mark prompting unleashes extraordinary visual grounding in gpt-4v. *arXiv preprint arXiv:2310.11441*, 2023. 4

Zhengyuan Yang, Zhe Gan, Jianfeng Wang, Xiaowei Hu, Faisal Ahmed, Zicheng Liu, Yumao Lu, and Lijuan Wang. Unitab: Unifying text and box outputs for grounded vision-language modeling. In *ECCV*, 2022. 9

Tianwei Yin, Xingyi Zhou, and Philipp Krähenbühl. Center-based 3d object detection and tracking. *CVPR*, 2021. 7, 8

Haoxuan You, Haotian Zhang, Zhe Gan, Xianzhi Du, Bowen Zhang, Zirui Wang, Liangliang Cao, Shih-Fu Chang, and Yinfei Yang. Ferret: Refer and ground anything anywhere at any granularity. *arXiv preprint arXiv:2310.07704*, 2023. 4, 9

Licheng Yu, Patrick Poirson, Shan Yang, Alexander C Berg, and Tamara L Berg. Modeling context in referring expressions. In *Computer Vision–ECCV 2016: 14th European Conference, Amsterdam, The Netherlands, October 11-14, 2016, Proceedings, Part II 14*, 2016. 7, 9

Licheng Yu, Zhe Lin, Xiaohui Shen, Jimei Yang, Xin Lu, Mohit Bansal, and Tamara L Berg. Mattnet: Modular attention network for referring expression comprehension. In *Proceedings of the IEEE conference on computer vision and pattern recognition*, pp. 1307–1315, 2018. 9

Hao Zhang, Hongyang Li, Feng Li, Tianhe Ren, Xueyan Zou, Shilong Liu, Shijia Huang, Jianfeng Gao, Lei Zhang, Chunyuan Li, and Jianwei Yang. Llava-grounding: Grounded visual chat with large multimodal models, 2023a. 9

Shilong Zhang, Peize Sun, Shoufa Chen, Min Xiao, Wenqi Shao, Wenwei Zhang, Kai Chen, and Ping Luo. Gpt4roi: Instruction tuning large language model on region-of-interest. *arXiv preprint arXiv:2307.03601*, 2023b. 4

A Training Details

In this section, we provide more training and implementation details of **Cube-LLM**.

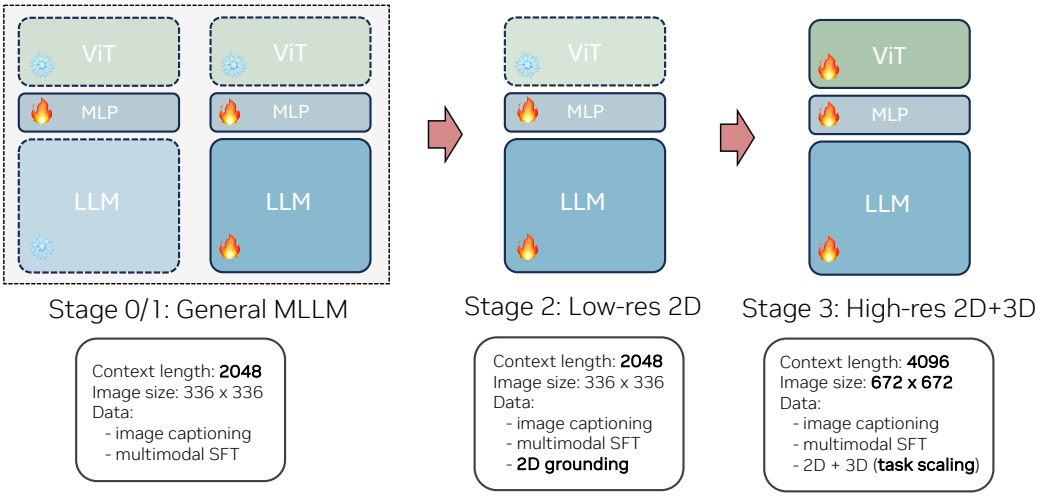

Figure 8: **Cube-LLM training pipeline.** We illustrate different stages of **Cube-LLM** training pipeline. Stage 0 and 1 follow common MLLM training following (Liu et al., 2023a), Stage 1 trains 2D parts of LV3D in low-resolution with the vision encoder frozen. Finally, we fully finetune on all 2D and 3D parts of LV3D in high-resolution (672×672). In Figure 5 (bottom right, second) we compare this setup to combining the Stage 2 and 3 together.

Implementation details. We use LLaVA-1.5 Liu et al. (2023a) with Vicuna-7B as our base model. We replace the CLIP visual encoder with ViT-L/14 Dosovitskiy et al. (2021) based DINOv2. For all localization outputs, we use 3 decimal places with text tokens, and keep 3 tokens per value (e.g., `[021,521, ...]`). Accordingly, we pre-process all LLaVA instruction-following data to reflect this change. We follow the same alignment step to train the MLP projection layers with the same training setup in Liu et al. (2023a). For 2D and 3D pretraining, we use random sampling following the sampling rate in Table 1. Each data sample (image-annotation pair) is converted to the multi-turn conversation format (Fig. 3) sampled at random. During pretraining, we use 8×8 A100s with a batch size of 1024 and train the model with a learning rate $lr = 2 \times 10^{-5}$ on images with 336×336 resolution. Then, we fine-tune all parameters including the visual encoder on a higher resolution 672×672 with 8×8 A100s and a batch size of 256 with 4 gradient accumulation steps (effective batch size of 1024) and a learning rate $lr = 2 \times 10^{-5}$.

CUBE-LLM pre-training undergoes the pretraining stage and finetuning stage. The pretraining is done on LV3D with the dataset multiples specified in Table 1 of the main paper. In this stage, all object depth z are transformed to align with the virtual camera (same practice as Omni3D Brazil et al. (2023)) and converted to log-scale. For each $(x, y, z, w, h, l, r_1, r_2, r_3)$, we normalize x and y in image coordinate from 0 to 999. For z, we set $z_{\text{min}} = -4$ and $z_{\text{max}} = 5$ (after log-scale) and rescale in 0 and 999. Similarly, $w_{\text{min}} = 0, w_{\text{max}} = 15, h_{\text{min}} = 0, h_{\text{max}} = 15, l_{\text{min}} = 0, l_{\text{max}} = 15$. All Euler angles are normalized between 0 and 2π. We train all 3 Euler angles in "yaw", "pitch", and "roll" order. Such ordering of angles in pretraining ensures consistent sequential ordering before and after finetuning. To support flexible question formats during inference, we prepare a set of question templates and randomly sample one per object during training (*e.g.*, "`Provide 3D bounding box of the region in the image that this sentence describes: <>`" or "`What is the 3D box of the <>?`"). For datasets where text does not contain orientation-specific information, we apply random horizontal flip data augmentation. We shuffle object order randomly, use all objects even if there are duplicate questions, and cut off the training token sequence by the context length of the language model (4096). We pre-train with 336×336 image size with frozen image-encoder and 672×672 with full training. Figure 8 illustrates the overal training pipeline of **CUBE-LLM**. This stage-wise training more beneficial compared to fully finetuning from beginning, as compared Figure 5 (bottom right).

CUBE-LLM fine-tuning undergoes a few change. Since finetuning benchmarks are all for outdoor scenes, we finetune z to be in meter (*i.e.,* no log-scale), and set $z_{\text{min}} = 0, z_{\text{max}} = 140$. We also ignore "pitch" and "roll" and only train for "yaw": (x, y, z, w, h, l, r_1). We finetune on Talk2Car, DriveLM-grounding, and NuScenes dataset altogether for 10 epochs. We randomly prompt ground-truth boxes in the system prompt to allow specialist prompting at inference. We also randomly sample to query either 2D bounding box, 3D bounding box, or 2D-to-3D multi-turn question answering.

B DATASET DETAILS

LV3D. Each data in LV3D is an image and annotation pair. Each annotation consists of a list of objects present in each image. Each object has a list of question and answer pairs as described in Section 3.2 of the main paper. If the data is from 2D dataset (*e.g.*, COCO), the question answer pairs include "`text` $\rightarrow$ `2D box`", "`2D center` $\rightarrow$ `2D box`", "`2D box` $\rightarrow$ `text`", *etc*. Similarly, if the data is from 3D dataset (*e.g.*, NuScenes), the question includes "`text` $\rightarrow$ `3D box`", "`2D center` $\rightarrow$ `3D box`", "`2D center` $\rightarrow$ `depth`", "`2D box` $\rightarrow$ `text`", *etc*., as discussed in the Section 3 of the main paper. To supplement text information, we leverage metadata from each dataset for each object class, such as object attribute in NuScenes dataset ("`pedestrian`" $\rightarrow$ "`a walking pedestrian.`"). For GRIT Peng et al. (2023), we used the subset of the first 500 folders, which is about $\frac{1}{3}$. AS Wang et al. (2024a) is a collection of VQA datasets as well as some machine-generated 2D grounding data from a subset of SegmentAnything-1B Kirillov et al. (2023). The original annotations contain a substantial amount of noise with duplicate answers. We simply remove the question-answer pairs of exactly identical and irrelevant answers. We also convert all the bounding boxes to follow the same format as **CUBE-LLM**. For data standardization, we follow Omni3D Brazil et al. (2023) and convert all datasets to a virtual camera of focal length $f = 512$.

Indoor 3D grounding benchmark. We use the testset of Objectron Ahmadyan et al. (2021), ArkitScenes Baruch et al. (2021), and SUN-RGBD Song et al. (2015) to evaluate the 3D grounding performance of **CUBE-LLM**. In particular, we show the impact of data scaling with a smaller subset of our pre-training dataset, LV3D-small. In LV3D-small, we remove the GRIT subset Peng et al. (2023), AS-filtered Wang et al. (2024a), Waymo Sun et al. (2020), Lyft Houston et al. (2021), Argoverse2 Wilson et al. (2021), while both LV3D and LV3D-small have the same amount of indoor datasets. To evaluate grounding performance, we measure precision at τ where $\tau \in [0.15, 0.25, 0.5]$. When an image contains more than one object associated with the input text prompt, we consider the max IOU. To augment object location to the text prompt, we add "`<object> close to camera`" if the depth is less than 0.8m. We add "`<object> on the left`" or "`<object> on the right`" if the object center is within the left/right 20 % of the image and the distance from the camera is 1/4/10 me away for small/medium/large objects. We define an object as small/medium/large by the max dimension (w, h, l), with a threshold of 0.5, 2, 3m. Similarly, we add "`<object> at the center`" if the object center is within the center 20 % and the distance from the camera is 1/4/10 m away for small/medium/large objects.

DriveLM-QA training. We aim to be consistent with the baseline training recipe Sima et al. (2023). We preprocess DriveLM questions and answers to follow the bounding box format of **CUBE-LLM**; 3 decimal places, normalized between 0 and 1. For both LLaVA and **CUBE-LLM**, we train on DriveLM-QA for 5 epochs. For both LLaVA and **CUBE-LLM**, we use image resolution of 336×336 and simply fed the 6 images independently to the vision encoder and concatenated them before feeding them to the language model. The number of vision tokens is 576×6 for each frame. We do not use any additional input (*e.g.*, previous frames or point cloud) to compare to the baselines although **CUBE-LLM** can enhance 3D perception with specialists. We hold out scene IDs:

`"64a3a2d22172406c848f2a92275808ba", "08be42eb2186411d8e2201225329f1c6",`

`"4b5bf3f4668d44fea9a676e9c4a8a79e", "0e247ba64b9d4a34a7256b6c173b1b5d",`

`"dbd9183e1278475ea54761297e004b04", "4098aaf3c7074e7d87285e2fc95369e0",`

`"9f3c8453d03d4df5946444757376b826", "2fc3753772e241f2ab2cd16a784cc680",`

`"d0880a386b6d434bb5cd13c134af7a3e", "01c3f5e39956402da3e37845632fadca"`

in *our split* evaluation.

DriveLM dataset comprises questions about *perception* (e.g., "what are the objects worth noting in the current scenario?"), *prediction* (e.g., "Where might the van, the sedan, and the pedestrian move in the future?), *planning* (e.g., "What are the safe actions of the ego car considering those objects?") and *behavior* (e.g., "what would the ego vehicle's next action would be?").

C TALK2CAR GROUNDING WITH VCOT.

Figure 9 visualizes our visual chain-of-thought prompting inference on Talk2Car images. For each image and text prompt, we first ask with question:

"`Please provide 2D bounding box of the region this sentence describes: <caption>.`".

Then, with the model prediction, we construct the second question as:

"`Please provide 2D bounding box of the region this sentence describes: <caption>.`"

`<2D bounding box>`

"`Please provide 3D bounding box of the region this sentence describes: <caption>.`" This simulates multi-turn conversation and the model can attend to the tokens of the previous conversation to infer the final output. We witness that as the text prompt becomes more complicated, the guidance of the 2D bounding box helps more.

D DRIVELM-QA VISUALIZATION

Figure 13, 14, and 15 show various types of DriveLM questions. A large portion of the questions asks about a particular object specified in `<object ID, camera name, x, y>` format. **CUBE-LLM** is capable of reasoning about the surrounding environment from the input multi-view images. When the **CUBE-LLM** and the ground truth do not align (*e.g.*, Figure 13 top and 15 bottom), it is evident that **CUBE-LLM** understands the overall layout of surrounding objects relative to the ego vehicle. Figure 16, 17 and 7 are the QA samples specifically for grounding important objects nearby. Notable points are that some of the objects that **CUBE-LLM** predicts that do not align with the ground truth (colored in red) are still important in each driving scenario. For example, in Figure 16 **CUBE-LLM** predicts a traffic sign (warning sign for crossroad), in Figure 17 **CUBE-LLM** predicts a white sedan in front right camera that the ego may need to pay attention to, and in Figure 7 **CUBE-LLM** predicts a white sedan in back camera.

E FAILURE CASES

In Figure 18 and 19, we show some failure cases of **CUBE-LLM** grounding result on DriveLM test set. **CUBE-LLM** makes incorrect prediction mainly in two reasons: *inaccurate depth* and *semantic mismatch*. Figure 18 shows three examples of inaccurate depth errors and Figure 19 shows three examples of semantic mismatch. Notably, for the inaccurate depth cases, the projected 3D boxes show accurate 2D localization in the image coordinate. This is because **CUBE-LLM** trains to connect its 2D understanding to 3D, as described in

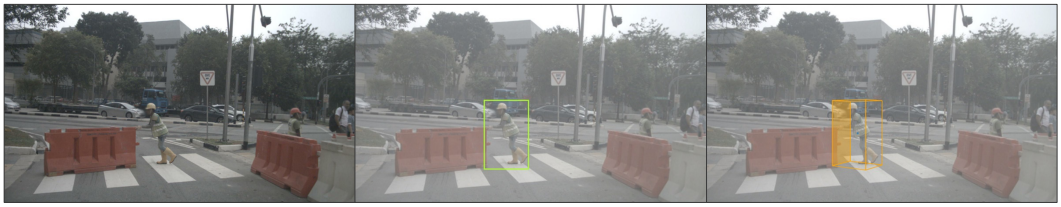

"Stop in front of the man in the yellow hat."

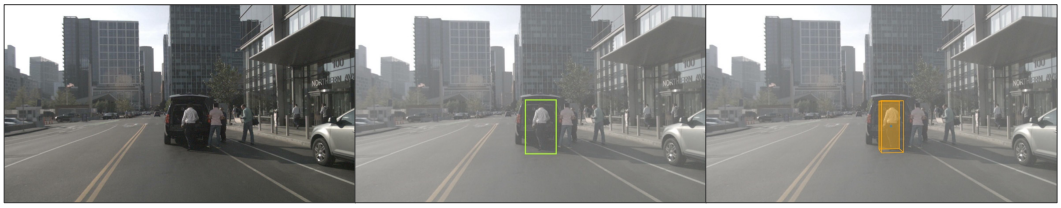

"Pull up behind the guy wearing a white shirt. He is my uncle."

"Turn left here, park behind the white van, left of the black car."

"Stop close to this bike so I can see if it is my friend's or not."

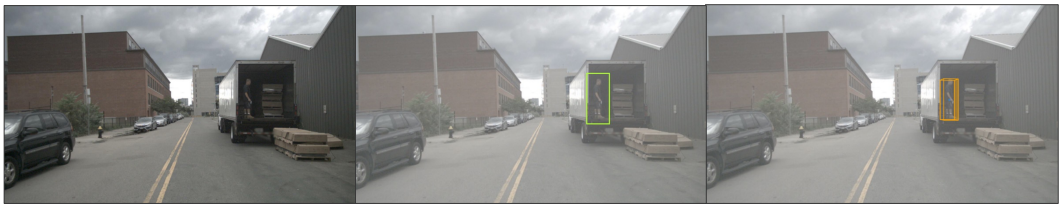

"Stop near Joe in the truck."

"Pull alongside the first barrier on the right."

Figure 9: **CUBE-LLM visual chain-of-thought prompting inference.** The first column is an input image, the second column is the 2D bounding box prediction, and the third column is the final 3D bounding box prediction prompted with the 2D prediction and text.

Section 3.3 of the main paper. For the semantic mismatch cases, **CUBE-LLM** struggles in correctly recognizing attributes when two similar objects are next to each other (*e.g.*, *silver sedan* vs. *white sedan*, *gray SUV* vs. *white SUV*). Similarly, Figure 21 and Figure 20 show the failure cases of **CUBE-LLM** on Talk2Car test set.

Figure 10: **CUBE-LLM visual prompting inference with specialist predictions.** First column is an input image, the second column is the specialist predictions (**blue**) and the ground truth (**orange**), and the third column is the final 3D bounding box prediction of **CUBE-LLM**.

Again, **CUBE-LLM** is still able to predict the accurate size and projected 2D box region. Figure 20 shows that **CUBE-LLM** struggles to recognize the correct color of the car under the shade, the physical status of the black car (moving vs parked), and does not understand "*closest to the curb*."

F LIMITATIONS

CUBE-LLM has several limitations. First, **CUBE-LLM** does not employ any resampling methods Dai et al. (2023); Alayrac et al. (2022) to reduce the number of vision tokens. This will limit the model to increase the input resolution to even larger than the current 672×672 (*e.g.*, 1344×1344). **CUBE-LLM** currently only supports a single frame input. However, video input is critical to correctly recognize the dynamics of the environment. As a result, **CUBE-LLM** tends to fail to correctly predict whether an object is stationary or moving, or rely on the

location of an object in the scene and infer the object's dynamics (*e.g.*, a car inside a parking space is most likely stationary). We leave these limitations for future work.

G SOCIETAL IMPACTS

The end results of this paper provide a foundation model for comprehensive reasoning tasks with 2D and 3D scene understanding. This is of use to a broad spectrum of applications including human-computer interaction, self-driving cars, robotics applications, and so on. In particular, it has the potential to improve the safety of these systems, as correctly grounding objects in the scene de-hallucinates the model's reasoning capability. Before deployment, appropriate safety thresholds must be cleared. Our approach does not specifically leverage dataset biases, although being a machine learning approach, it is impacted as much as other machine learning techniques.

Figure 11: **More visualization of 3D grounding. CUBE-LLM** is capable of grounding object with spatial cues and understand complex questions.

Figure 12: **More visualization of 3D grounding.** **CUBE-LLM** is capable of grounding open-vocabulary category names.

Question: What actions taken by the ego vehicle can lead to a collision with **<c1,CAM_FRONT_RIGHT,190.8,660.8>**?

Cube-LLM: Slight right turn.

Ground Truth: Moderate right turn.

Question: What is the moving status of object **<c1,CAM_BACK_LEFT,740.8,428.3>**? Please select the correct answer from the following options: A. Back up. B. Turn left. C. Stopped. D. Turn right.

Cube-LLM: B. Turn left.

Ground Truth: B

Figure 13: **CUBE-LLM prediction on DriveLM-QA.** Green marks are the reference marks and the corresponding bounding box in the question. Orange marks are predicted 2D points by **CUBE-LLM**. Blue marks are the reference marks and the corresponding bounding box in the ground truth answers.

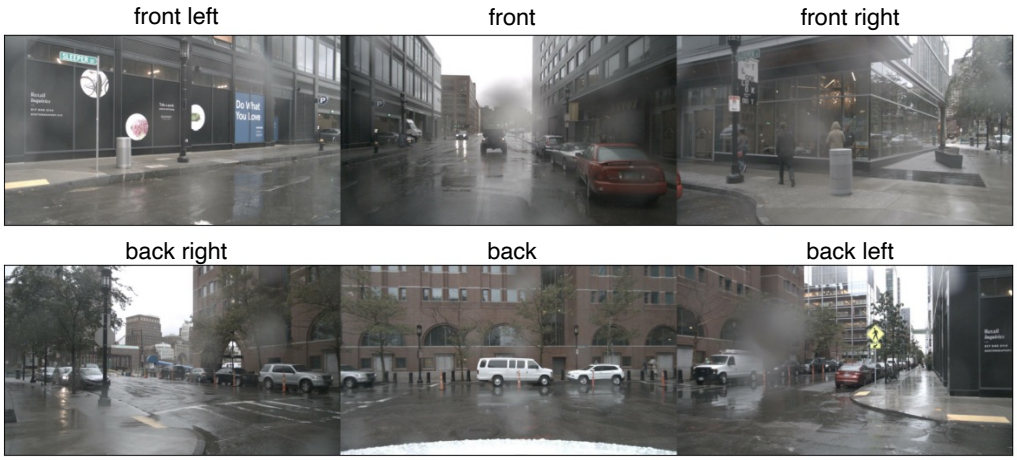

Question: Predict the behavior of the ego vehicle. Please select the correct answer from the following options: A. The ego vehicle is going straight. The ego vehicle is driving very fast. B. The ego vehicle is steering to the left. The ego vehicle is driving very fast. C. The ego vehicle is slightly steering to the right. The ego vehicle is driving fast. D. The ego vehicle is going straight. The ego vehicle is driving with normal speed.

Cube-LLM: D. The ego vehicle is going straight. The ego vehicle is driving with normal speed.

Ground Truth: D

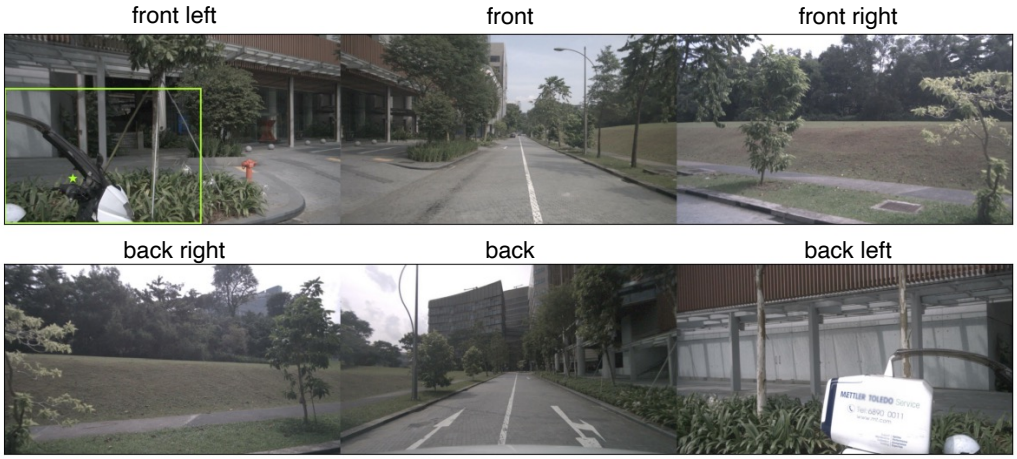

Question: What actions taken by the ego vehicle can lead to a collision with **<c2,CAM_FRONT_LEFT,327.2,684.3>**?

Cube-LLM: Slight left turn.

Ground Truth: Slight left turn.

Figure 14: **CUBE-LLM prediction on DriveLM-QA.** Green marks are the reference marks and the corresponding bounding box in the question. Orange marks are predicted 2D points by **CUBE-LLM**. Blue marks are the reference marks and the corresponding bounding box in the ground truth answers.

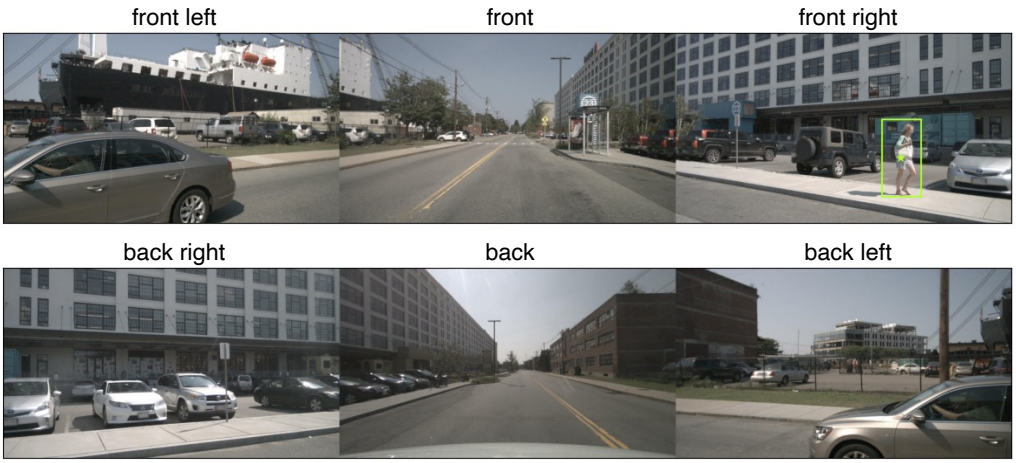

Question: What is the moving status of object **<c2,CAM_FRONT_RIGHT,1068.3,591.7>**? Please select the correct answer from the following options: A. Turn right. B. Stopped. C. Reverse parking. D. Going ahead.

Cube-LLM: D. Going ahead.

Ground Truth: D

Question: What actions taken by the ego vehicle can lead to a collision with **<c2,CAM_BACK,1285.8,596.7>**?

Cube-LLM: Reversing to the left rear can lead to a collision with **<c2,CAM_BACK,1286.4,596.7>**.

Ground Truth: Changing to the left lane.

Figure 15: **CUBE-LLM prediction on DriveLM-QA.** Green marks are the reference marks and the corresponding bounding box in the question. Orange marks are predicted 2D points by **CUBE-LLM**. Blue marks are the reference marks and the corresponding bounding box in the ground truth answers.

Question: What object should the ego vehicle notice first when the ego vehicle is getting to the next possible location? What is the state of the object that is first noticed by the ego vehicle and what action should the ego vehicle take? What object should the ego vehicle notice second when the ego vehicle is getting to the next possible location? What is the state of the object perceived by the ego vehicle as second and what action should the ego vehicle take? What object should the ego vehicle notice third? What is the state of the object perceived by the ego vehicle as third and what action should the ego vehicle take?

Cube-LLM: Firstly, notice that **<c3,CAM_FRONT,1257.6,656.1>**. The object is a traffic sign, so the ego vehicle should slow down and proceed. Secondly, notice that **<c1,CAM_FRONT,227.2,506.7>.** The object is going ahead, so the ego vehicle should continue going ahead at the same speed. Thirdly, notice that **<c2,CAM_BACK,1115.2,557.1>.** The object is going ahead, so the ego vehicle should continue going ahead at the same speed.

Ground Truth: Firstly notice that **<c1,CAM_FRONT,232.5,528.3>.** The object is going ahead, so the ego vehicle should keep going ahead at the same speed. Secondly notice that **<c2,CAM_BACK_LEFT,1228.3,611.7>.** The object is stationary, so the ego vehicle should keep going ahead at the same speed. Thirdly notice that **<c3,CAM_BACK,1126.7,549.2>.** The object is going ahead, so the ego vehicle should keep going ahead at the same speed.

Figure 16: **CUBE-LLM prediction on DriveLM-QA.** Green marks are the reference marks and the corresponding bounding box in the question. Orange marks are predicted 2D points by **CUBE-LLM**. Blue marks are the reference marks and the corresponding bounding box in the ground truth answers. Red circle is the predicted object that do not agree with the ground truth.

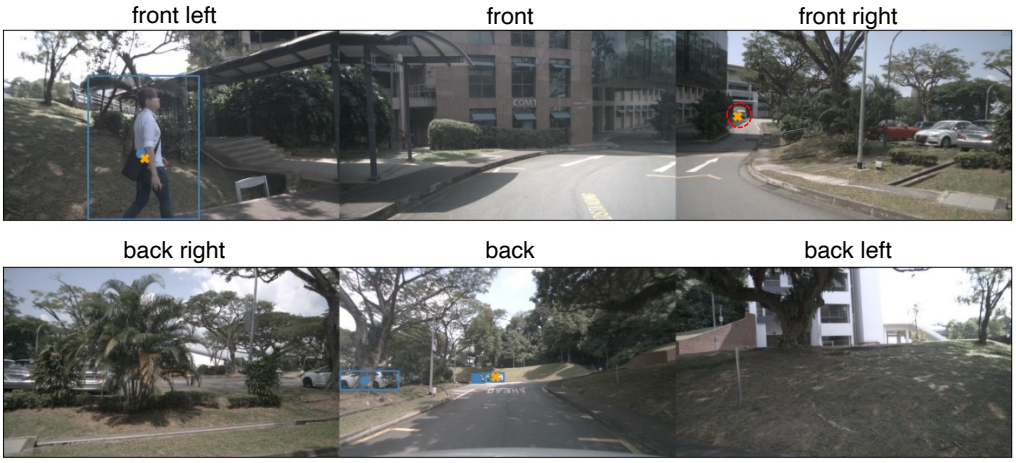

Question: What are the important objects in the current scene? Those objects will be considered for the future reasoning and driving decision.

Cube-LLM: There is a white sedan to the back of the ego vehicle, a man wearing a white shirt to the front left of the ego vehicle, and a white sedan to the front right of the ego vehicle. The IDs of these objects are **<c1,CAM_BACK,742.4,521.1>, <c2,CAM_FRONT_LEFT,673.6,609.3>**, and **<c3,CAM_FRONT_RIGHT,294.4,410.4>**.

Ground Truth: There is a white car to the back of the ego vehicle, a white clothes pedestrian to the front left of the ego vehicle, a white car to the back of the ego vehicle, and a black car to the back of the ego vehicle. The IDs of these objects are **<c1,CAM_BACK,731.7,525.8>, <c2,CAM_FRONT_LEFT,654.9,585.7>, <c3,CAM_BACK,120.0,539.2>,** and **<c4,CAM_BACK,655.0,529.2>.**

Figure 17: **CUBE-LLM prediction on DriveLM-QA.** Green marks are the reference marks and the corresponding bounding box in the question. Orange marks are predicted 2D points by **CUBE-LLM**. Blue marks are the reference marks and the corresponding bounding box in the ground truth answers. Red circle is the predicted object that does not agree with the ground truth.

"Elderly person in a floral shirt, moving."

"White pickup truck, stationary."

"Blue and white truck, stationary."

Figure 18: **Failure cases of DriveLM-Grounding images.** The error mainly attributes to incorrect depth. Each row has the original image (left), projected 3D box prediction and ground truth (middle), and BEV image (right). Blue box is the ground truth and Orange box is the prediction. In BEV images, Green box is the ground truth and red box is the prediction.

"White car, stationary."

"Silver sedan, stationary."

"White SUV, moving."

Figure 19: **Failure cases of DriveLM-Grounding images.** The error mainly attributes to semantic mismatch. Each row has the original image (left), projected 3D box prediction and ground truth (middle), and BEV image (right). Blue box is the ground truth and Orange box is the prediction. In BEV images, Green box is the ground truth and red box is the prediction.

"Once the light turns green, turn left behind the silver car."

"There is a red truck parked in a parking lot on the left hand side. Get over there."

"Stop next to my colleague who is standing on the right side of the road."

Figure 20: **Failure cases of Talk2Car images.** The error mainly attributes to incorrect depth. Each row has the original image (left), projected 3D box prediction and ground truth (middle), and BEV image (right). Blue box is the ground truth and Orange box is the prediction. In BEV images, Green box is the ground truth and red box is the prediction.

"Once the light turns green, turn left behind the silver car."

"Switch to right lane and park on right behind parked black car."

"My friend is the guy standing closest to the curb, next to that car in front of us. Pull over so he can get in."

Figure 21: **Failure cases of Talk2Car images.** The error mainly attributes to semantic mismatch. Each row has the original image (left), projected 3D box prediction and ground truth (middle), and BEV image (right). Blue box is the ground truth and Orange box is the prediction. In BEV images, Green box is the ground truth and red box is the prediction.